Multipass Welding Stresses in Very Thick Plates and Their Reduction from Stress Relief Annealing†

Yukio UEDA*, Eiji TAKAHASHI**, Keiji FUKUDA***, Koichi SAKAMOTO** and Keiji NAKACHO****

Abstract

An investigation into residual stresses induced in a connection of a pressure vessel by multipass welding and their reduction by stress relief annealing was conducted. The study was performed theoretically and experimentally on idealized research models. In the theoretical analyses, the thermal elastic-plastic creep theory developed by the authors was applied and the results of the analysis show a good, fundamental coincidence with the experimental findings.

The outline of the results and the conclusions is as follows.

(1) The largest transverse transient stress (σ_x) during welding always appears just below the weld metal of the newest layer. But as the layers of weld metal are piled up, this stress is relieved gradually. This implies that the application of intermediate annealing for the sole purpose on reducing welding residual stresses is unnecessary.

(2) In the welding residual stress (σ_x) distribution, the location of the largest tensile stress is just below the finishing bead. Judging from the residual stresses and available information about cracks in actual structures, delayed cracks do not initiate at the toe of weld on the surface, but do initiate several layers below it.

(3) The effectiveness of stress relief annealing depends greatly on the annealing temperature in the case of comparatively low heating rate for annealing.

1. Introduction

The demand for a large capacity in nuclear reactors and chemical plants requires the use of high quality thick plates for pressure vessels, which are the main structural components of these plants.

In the usual process of construction, multipass welding and stress relief annealing are utilized. These kinds of treatments may produce cold cracks and/or cracks due to stress relief annealing (SR cracks). Most crack surfaces are parallel to the weld lines. These cracks may propagate and damage the pressure vessel during trial or actual operation. In connection with this, problems related to residual stresses in the welded joints, especially in the direction perpendicular to the weld lines, should be investigated, since very few relevant papers can be found.

In this paper, residual stresses induced in welded joints between the cylinder and the head of the vessel will be investigated both experimentally and theoretically. The experiment will be conducted on idealized models with several different thicknesses. The residual stresses will be measured after completion of the welding process or after the stress relief annealing. For the theoretical analysis of the entire history of producing and relieving residual stresses, thermal elastic-plastic creep analysis developed by the authors will be applied.[1),2),3),4)]

2. Measurement of residual stresses

2-1 Idealization of the cylinder-head connection of a pressure vessel

A pressure vessel as shown in Fig. 1 (a) is axisymmetrical. Thus, the welding contraction induced in a circumferential joint between the cylinder and the head can be divided into the transverse shrinkage in the axial direction and the angular distortion along the weld line. The restraint against the former becomes more severe as the layers of weld are accumulated. There is hardly any angular distortion produced, even at the preliminary stage of welding, due to the high degree of internal structural restraint. Considering these restraining conditions, the joint is idealized as illustrated in Fig. 1 (b). This model is triaxially symmetric with respect to X, Y and Z axes. Each pass of weld is laid alternately on each side of the groove.

† Received on Sep. 16, 1976

* Professor

** Researcher, Central Research Laboratory, Kobe Steel Co., Ltd.

*** Research Associate

**** Graduate Student, Osaka University

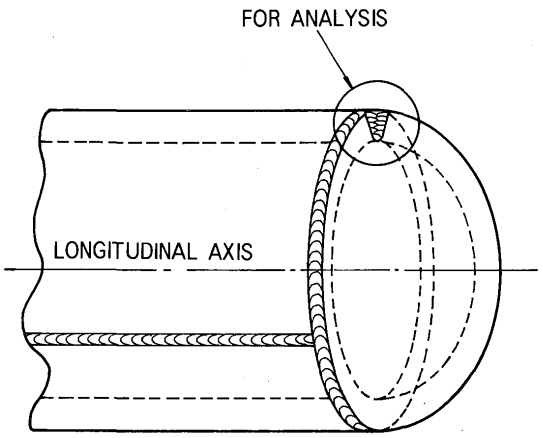

Fig. 1 (a) Welded cylinder-head connection of a pressure vessel

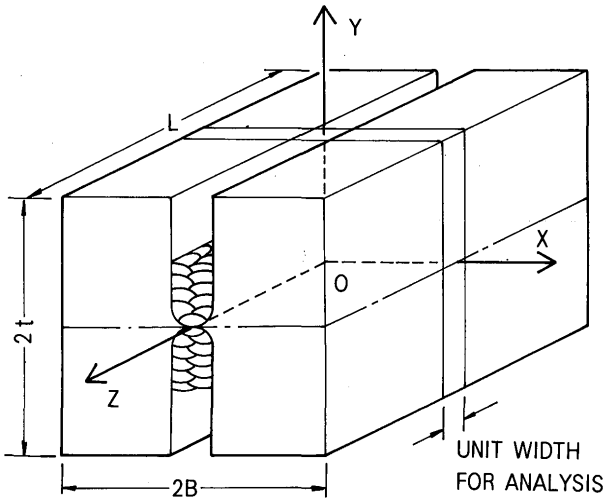

Fig. 1 (b) Idealized research model

Table 1 Chemical compositions and mechanical properties of 2¼Cr-1Mo Steel

Name of specimen	Chemical compositions (wt%)							Tensile properties		Thickness of plate (mm)	Heat treatment
	C	Si	Mn	P	S	Cr	Mo	Y.P. (kgf/mm²) *	T.S. (kgf/mm²)		
M-100	0.09	0.29	0.46	0.040	0.013	2.38	1.03	37.8	54.9	100	Normalized
M-200	0.11	0.22	0.47	0.007	0.011	2.03	1.01	31.5	53.7	200	〃
M-300	0.12	0.22	0.50	0.010	0.011	2.28	0.98	36.0	54.7	300	〃
Weld metal (US521A×MF29A)	0.07	0.42	0.78	0.012	0.012	2.28	1.06	71.5	80.7	—	—

* 1kgf/mm² = 9.8MN/m²

Table 2 Conditions of welding

Name of specimen	Current (A)	Voltage (V)	Velocity (cm/min.)	Heat-input (J/cm)	Preheating & interpass temp. (℃) *	Total number of passes	Total number of layers
M-100	600	35	28	45,000	200	7×2	7×2
M-200	550	34	33	34,000	200	43×2	20×2
M-300	650	34	27	49,111	200	83×2	34×2

* y=x+273, (y [K], x [℃])

The material of the model is ASTM A336F22 (2¼Cr-1Mo) and the chemical compositions and mechanical properties are listed in Table 1. The wire used for welding is US521A×MF29A (made by Kobe Steel Co., Ltd.).

2-2 Experimental method

For measurements of welding residual stresses, three models (M-100, M-200 and M-300) are furnished, being 100, 200 and 300 mm in thickness (2t), respectively. Submerged arc welding method is applied and welding conditions for each model are shown in Table 2.

Next, for stress relief annealing, two long pieces of M-200 are constructed. Both are then cut into three pieces each. The cuts are made perpendicular to the weld line. Two of these pieces are 30 mm wide and are cut from the center of the weld line. They are used for measurements of welding residual stresses. The other four, models

Table 3 Conditions of stress relief annealing

Name of specimen	Thickness of plate (mm)	Heating & cooling rate (℃/hr.)	Heating temp. (℃)	Holding time (hr.)
MSR-200-1	200	30	600	0
MSR-200-2	200	30	650	0
MSR-200-3	200	100	650	0 *
MSR-200-4	200	30	650	4

* 1hr. holding is provided in the analysis. (ref. Fig. 13)

MSR-200-1, 2, 3 and 4, are supplied for stress relief annealing tests. Conditions of annealing are indicated in Table 3.

Adopting the sectioning method, residual stressec are measured on models cooled after welding or annealing. The measurements are made on the top surface and on the cross section newly exposed by making cuts 20 or 30 mm wide perpendicular to the weld line at the middle of it. The stress state of the middle of the model is in three dimensions before the cutting, and in two dimensions after the cutting because the longitudinal residual stresses (σ_Z) are relieved by the cutting. The residual stresses on the top surface are measured in both stress states. The ones on the cross section are measured only in the plane stress state because strain gages can be put on the cross section only after the cutting mentioned above.

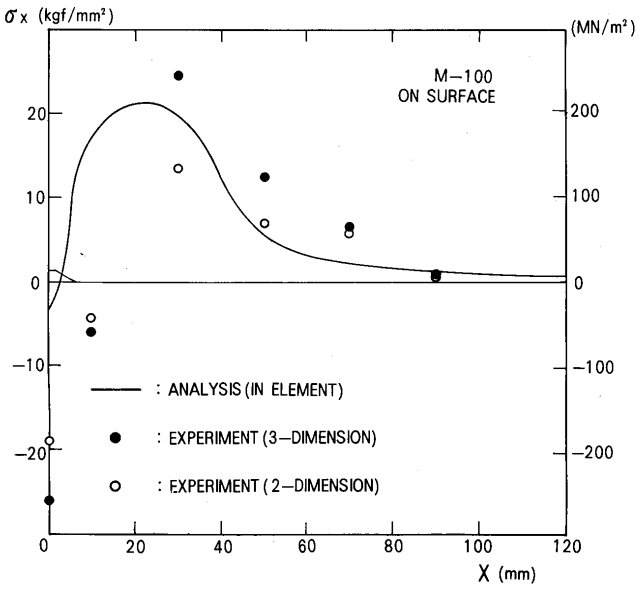

Fig. 3 (a) Transverse welding residual stresses (σ_X) on the top surface (M-100)

2-3 Observed residual stresses

2-3-1 Residual stresses due to welding

Observed longitudinal welding residual stresses (σ_Z) on the top surface of specimens M-100, M-200 and M-300 are indicated in Fig. 2.

Figs. 3 (a), (b) and (c) show experimental transverse welding residual stresses (σ_X) on the top surface in the middle of the weld line, and theoretical values which will be mentioned in the following chapter are illustrated with solid lines. Observed transverse welding residual stresses (σ_X) at the cross section are shown in Figs. 4 (a), (b), (c), (d) and (e). (Fig. 4 (b) includes the experimental results which were measured in the region of the HAZ.)

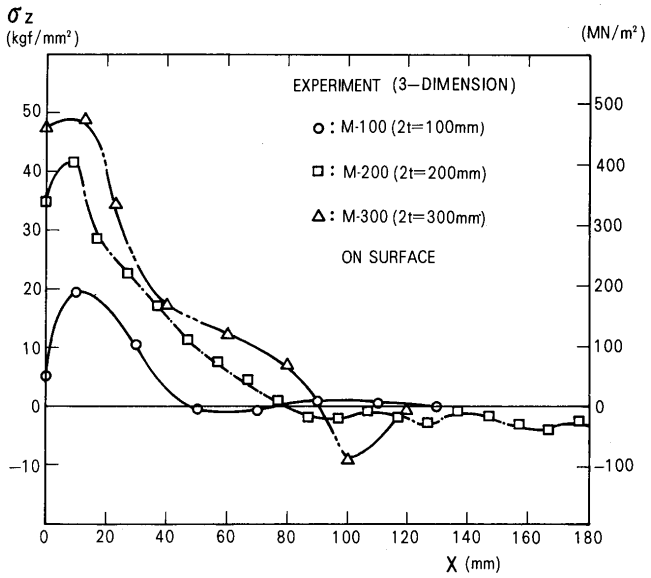

Fig. 2 Experimental longitudinal welding residual stresses (σ_Z) on the top surface (M-100, M-200, M-300)

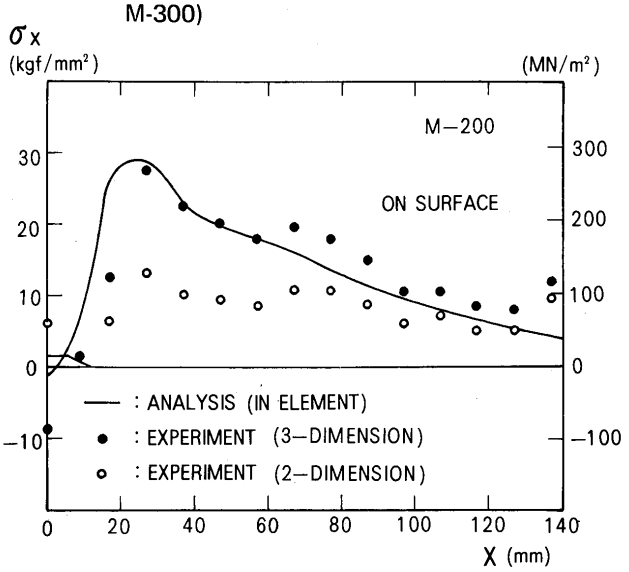

Fig. 3 (b) Transverse welding residual stresses (σ_X) on the top surface (M-200)

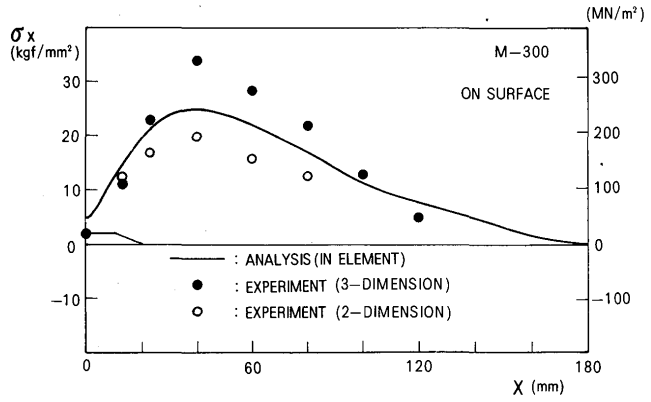

Fig. 3 (c) Transverse welding residual stresses (σx) on the top surface (M-300)

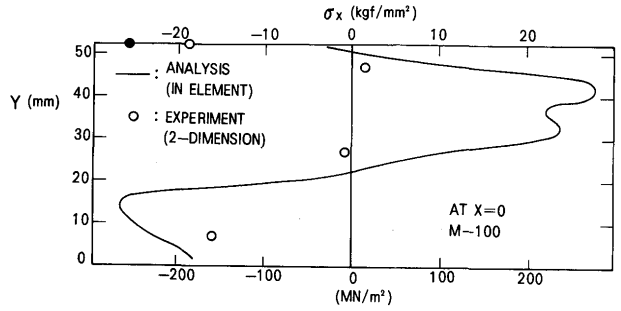

Fig. 4 (a) Transverse welding residual stresses (σ_X) at the cross section (M-100, AT X = 0)

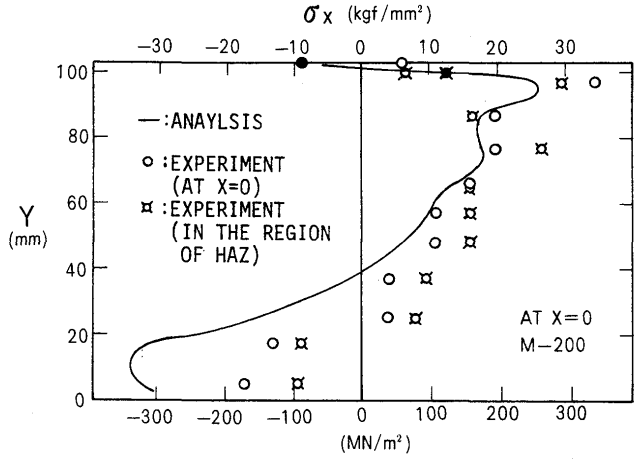

Fig. 4 (b) Transverse welding residual stresses (σ_X) at the cross section (M-200, AT X = 0)

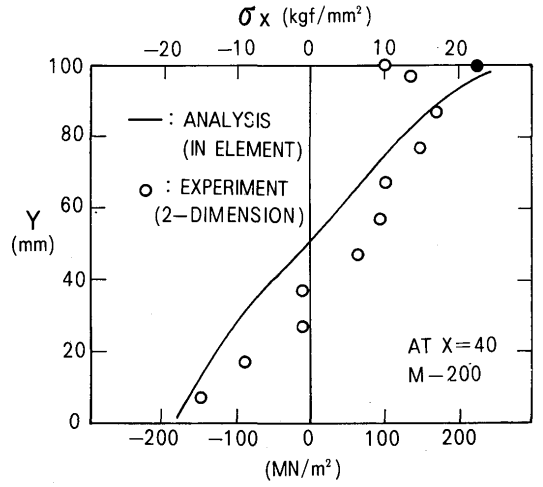

Fig. 4 (c) Transverse welding residual stresses (σ_X) at the cross section (M-200, AT X = 40)

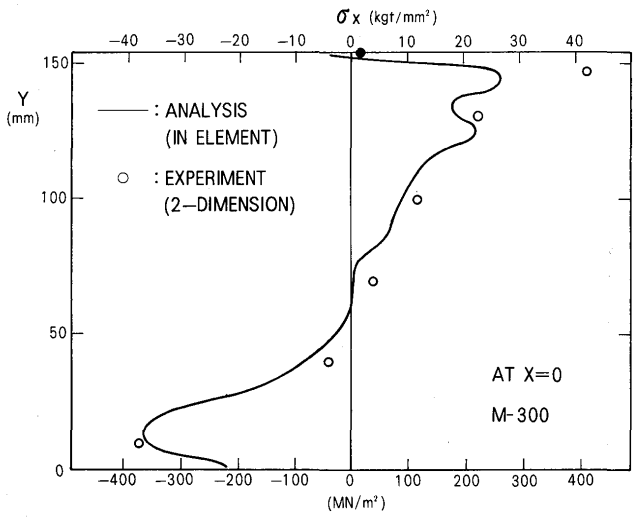

Fig. 4 (d) Transverse welding residual stresses (σ_X) at the cross section (M-300, AT X = 0)

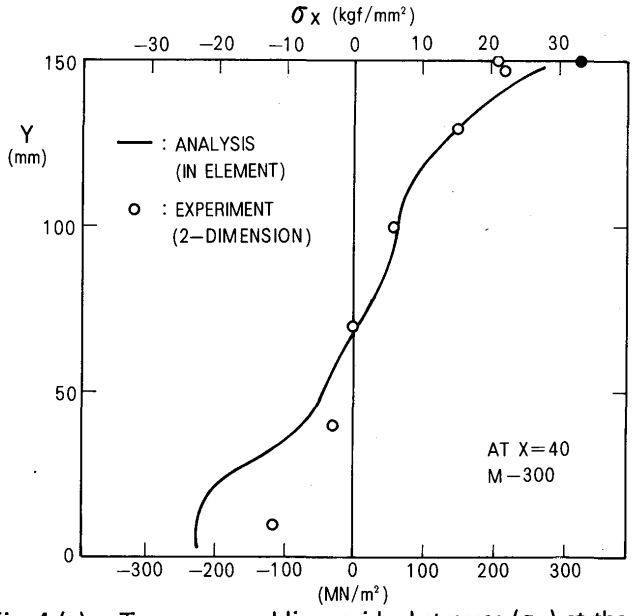

Fig. 4 (e) Transverse welding residual stresses (σ_X) at the cross section (M-300, AT X = 40)

2-3-2 Residual stresses after annealing

Residual stresses are measured on four MSR-200 models after annealing under four different conditions. Longitudinal residual stresses (σ_Z) and transverse residual stresses (σ_X) on the top surface in the middle of the weld line are represented in Figs. 5 and 6, respectively. Transverse residual stresses (σ_X) at the cross section are also shown in Figs. 7 (a) and (b).

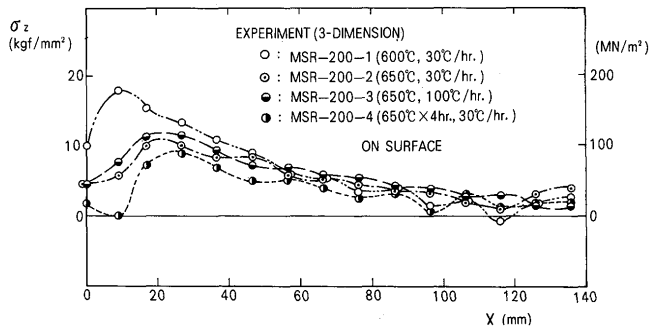

Fig. 5 Experimental longitudinal residual stresses (σ_Z) after annealing on the top surface (MSR-200-1, 2, 3, 4)

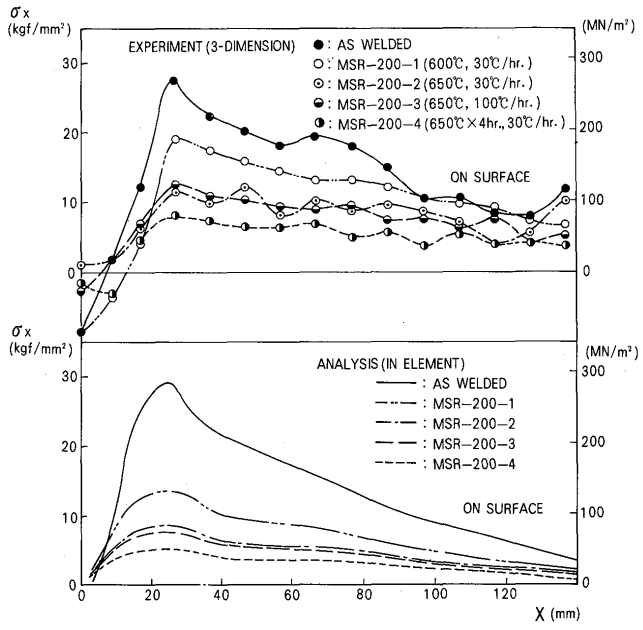

Fig. 6 Transverse residual stresses (σ_X) after annealing on the top surface (MSR-200-1, 2, 3, 4)

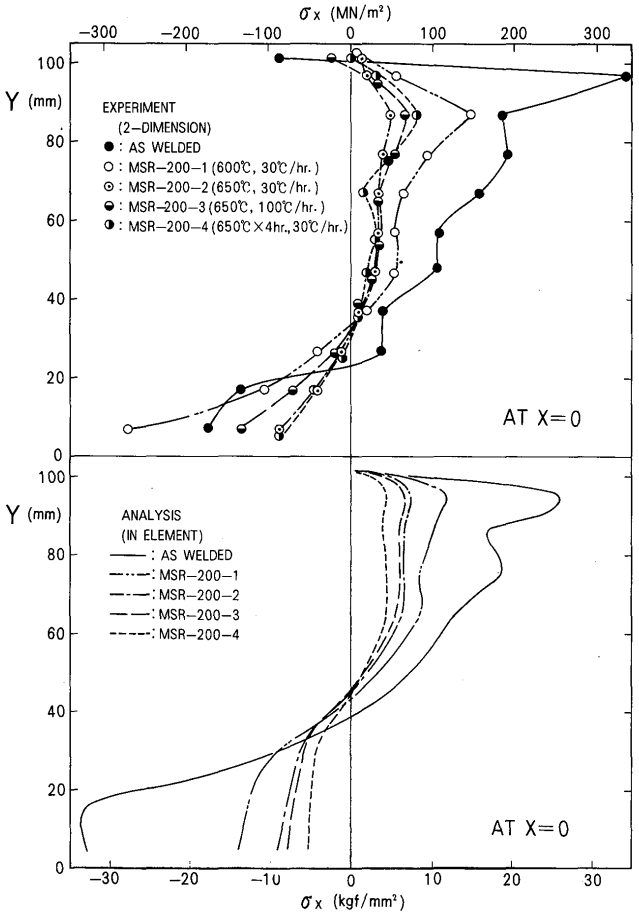

Fig. 7 (a) Transverse residual stresses (σ_X) after annealing at the cross section (MSR-200-1, 2, 3, 4, AT X = 0)

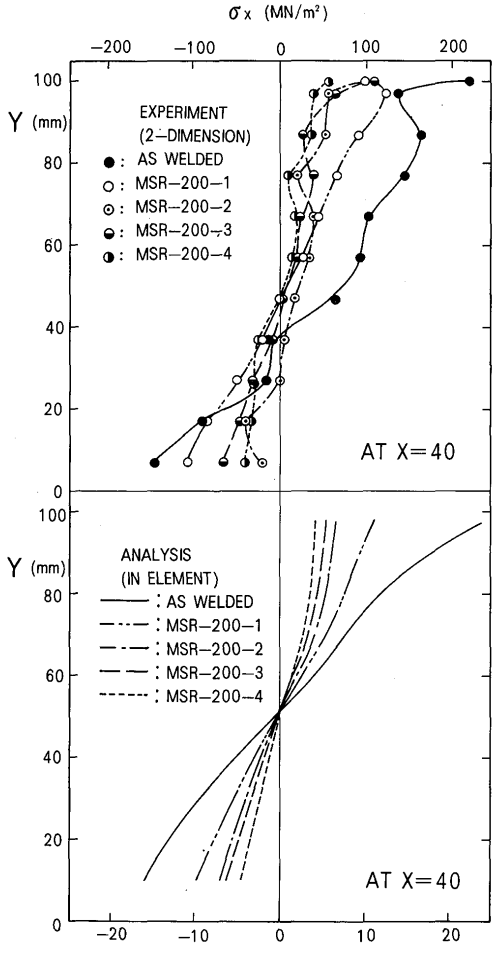

Fig. 7 (b) Transverse residual stresses (σ_X) after annealing at the cross section (MSR-200-1, 2, 3, 4, AT X = 40)

3. Thermal stress analyses for multipass welds and SR treatment

The authors have already developed the theory of thermal elastic-plastic creep analysis based on the finite element method for analysing the mechanical phenomenon observed not only during welding but also during stress relief annealing. This method can take into account the temperature dependency of mechanical properties (e.g. yield stress, Young's modulus, coefficient of linear expansion, creep properties, etc.).

Heat conduction analysis is conducted by the finite difference method.

3-1 Material constants used in the analyses

3-1-1 Physical properties in heat conduction analysis

Temperature dependent physical properties of the material used in the heat conduction analysis are shown in Fig. 8. These are density (γ), specific heat (c), heat conductivity (λ) and heat transfer coef. (a). These properties are determined from test results conducted in this study, in addition to information already available for similar materials.

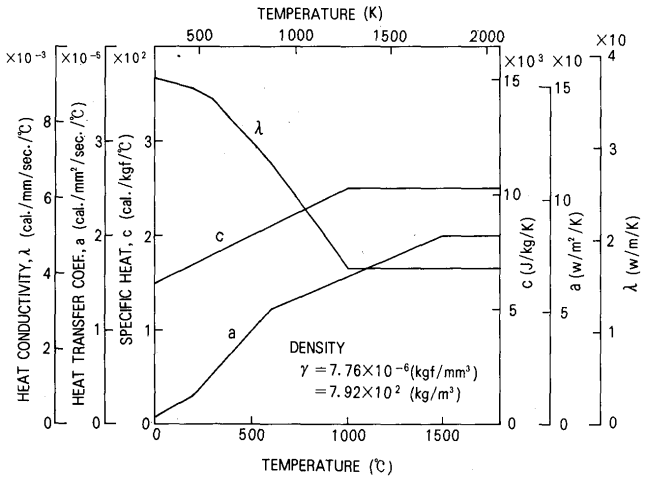

Fig. 8 Physical properties used in heat conduction analysis

3-1-2 Mechanical properties in thermal stress analysis

To idealize the mechanical properties, the following assumptions are made, taking into account the preliminary test results.

(1) Phase transformations occur instantaneously at a specific temperature.

(2) Austenite phase transformation in the heating stage starts at a temperature of 750°C (which is the average temperature of Ac_1 and Ac_3), and the metals reveal no tendency to show resistance above that temperature.

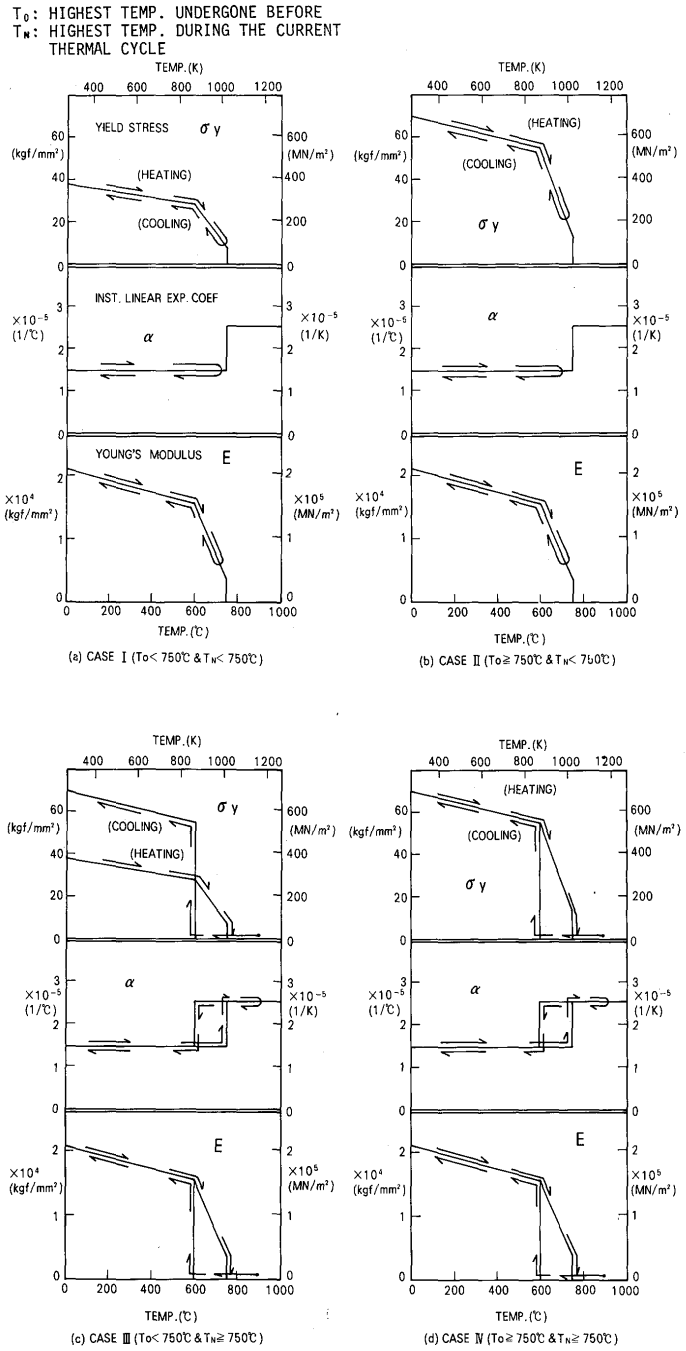

Fig. 9 Mechanical properties used in thermal stress analysis

(3) Phase transformation in the cooling stage starts at a temperature of 600°C (which is the average temperature of Bs and Ms). Above this temperature, weld metal and HAZ reveal no resistance.

(4) The metals are elastic and perfectly plastic materials.

Based on the above assumptions, the mechanical properties used in the analysis are idealized as illustrated in Fig. 9, which change according to the thermal history of the material undergone.

3-1-3 Creep properties at high temperature

Parameters in the following strain-hardening creep law are determined from creep test results, as shown in Fig. 10 (a).

$$\dot{\varepsilon}^c = mA^{\frac{1}{m}} \sigma^{\frac{\gamma}{m}} (\varepsilon^c)^{1-\frac{1}{m}} \quad (1)$$

Arranging the creep strain rates of the steady state in the experiment, according to the following power creep law, the constants n and β are represented in Fig. 10 (b).

$$\dot{\varepsilon}^c = \beta \sigma^n \quad (2)$$

Next, relaxation test results at constant temperature are shown in Fig. 11. The solid lines in Fig. 11 are calculated by the strain-hardening creep law with the constants

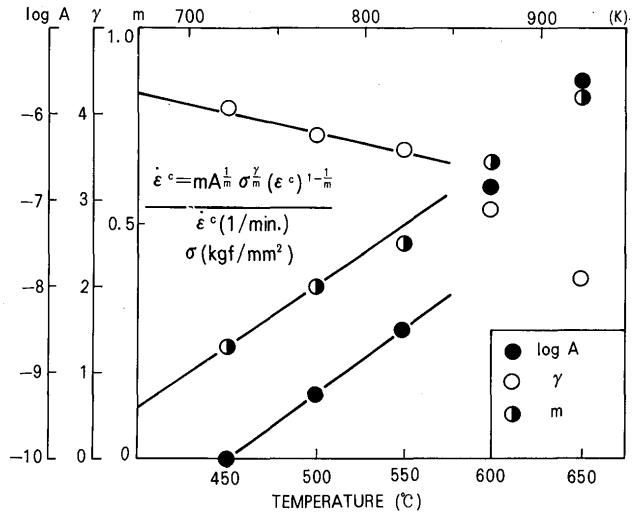

Fig. 10 (a) Observed values of constants in the strain-hardening creep law

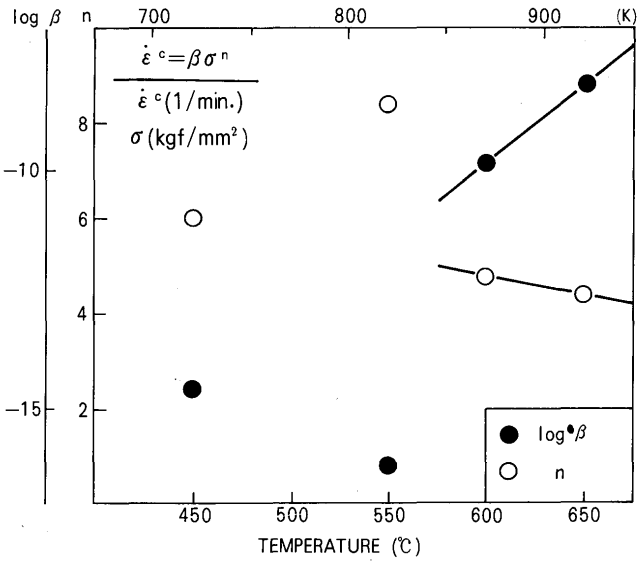

Fig. 10 (b) Observed values of constants in the power creep law

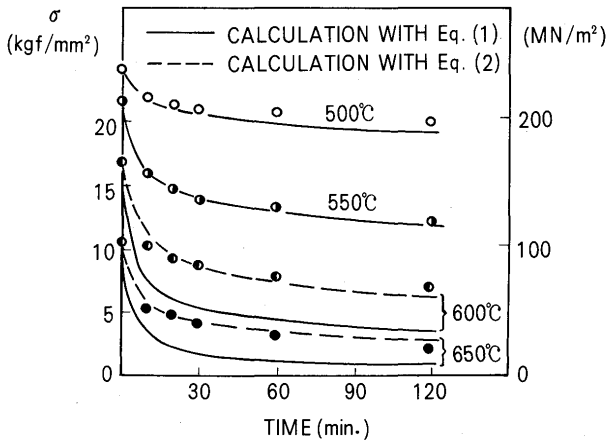

Fig. 11 Relaxation test results at constant temperature

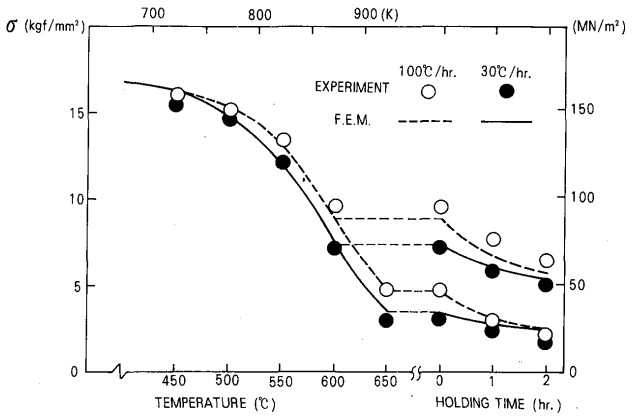

Fig. 12 Results of stress relaxation during heating and holding stages

in Fig. 10 (a). On the other hand, the broken lines represent the results calculated by the power creep law using the constants in Fig. 10 (b). Based on these results, it is assumed in the following analysis that the creep strain rate below 575°C obeys the strain-hardening creep law and the one above 575°C obeys the power creep law. (In the case of the strain-hardening creep law, a special method for analysis may be necessary. The method and the procedure will be discussed in Appendix I.)

In order to examine this assumption, analyses of stress relaxation during heating and holding stages are conducted at the heating rates of 100°C/hr. and 30°C/hr.. The results are represented in Fig. 12 in comparison with the experimental results, respectively. Both results coincide. This fact confirms the appropriateness of the above assumption.

3-2 Methods of analyses

The analyses are performed on the quarter of the specimens with unit lengths of weld line because the models are triaxially symmetric. The heat conduction

analysis is performed for each pass with an instantaneous heat source, and the thermal stress analysis is for the plane stress state.

In the case of very thick plates, the number of passes is very large, and if the analysis of all passes were performed, the time required for calculation would be enormous. According to preliminary calculation on specimen M-100, it is known that if the heat conduction analysis is performed for all passes and the thermal stress analysis is carried out on the last pass of each layer of the analysis, this approximate calculation can be conducted without loss of accuracy.

It is, of course, taken into account in the analysis that in the region of HAZ by the newest pass (which will be termed new HAZ in this paper), the stresses produced before the newest pass are released completely.

By the simplified analysis, the welding is reduced to 5 layers, 10 layers and 17 layers for specimens M-100, M-200 and M-300, respectively.

The conditions of annealing are indicated in Table 3. The holding time of specimen MSR-200-3 alone is one hour longer than that of the experiment. This is due to the fact that as represented in Fig. 13, the case of the heating rate of 100°C/hr. in the experiment requires one extra hour for the temperature of the specimen to reach the prescribed one when the temperature is close to it.

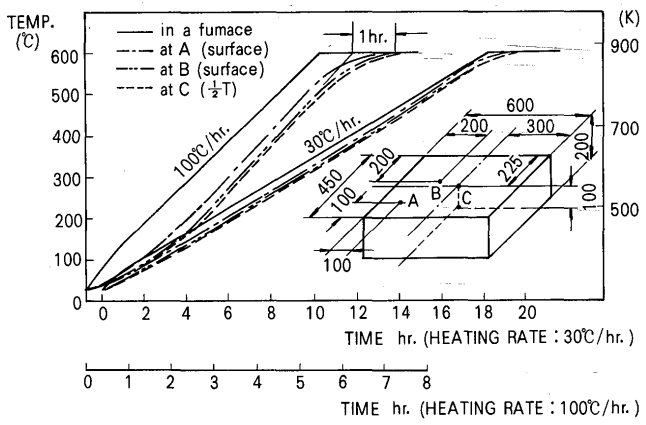

Fig. 13 Histories of temperature of a specimen during heating and holding stages

3-3 Theoretical residual stresses

3-3-1 Residual stresses due to welding

Transverse welding residual stresses (σ_X) on the top surface and at the cross section are shown in Figs. 3 and 4, respectively, compared with the measured results.

The stress distributions on the top surfaces obtained by theoretical analysis lie between two-dimensional experimental values and three-dimensional ones. This indicates that the theoretical results show a good coincidence with the experimental results except in the neighborhood of the weld metal of specimen M-100. In regard to the residual stresses on the cross sections of the specimens, both theoretical and experimental results coincide without exception.

3-3-2 Residual stresses after annealing

For residual stresses (σ_X) after the annealing, the theoretical values and the measured ones are represented in Figs. 6 and 7. The magnitudes of the transverse residual stresses on the top surface of the specimen obtained by theoretical analysis indicate a tendency according to the conditions of the annealing as follows;

(MSR-200-1) > (MSR-200-2)
$\cong$ (MSR-200-3) > (MSR-200-4)

The same tendency is also observed in the measured values. Concerning the absolute value of stress, the theoretical values are somewhat smaller than the experimental ones. This is attributed to the fact that the theoretical values are obtained by the analysis in the plane stress state, while the experimental values are measured in the three-dimensional stress state, similar to those due to welding.

In contrast with this, the theoretical stresses on the cross section of the specimen are well correlated with the experimental ones under all annealing conditions.

Good coincidence of these results including the welding residual stresses confirms validity of the method adopted for this study in spite of the idealizations and simplifications.

4. Considerations

4-1 Transient stresses and intermediate annealing

Taking specimen M-300 as an example, transverse transient and resulting residual stress (σ_X) distributions on the top surface and the cross section of the specimen are shown in Figs. 14 (a) and (b) respectively, (the transient stresses imply ones at the interpass temperature).

On the top surface of the specimen, the stresses increase gradually with progress of the welding. In the weld metal of the newest layer, tensile stress is produced, but the largest stress in the cross section appears just below it. This is also the largest in the whole specimen. The tensile stress in the weld metal (along the Y axis) is relieved as the subsequent passes are piled up, and it turns into compression in the weld metal that was laid at the earlier stage.

In the process of construction of a pressure vessel of this type, intermediate annealing is customarily provided several times. This treatment is expensive and time consuming. If this is required only for reduction of welding

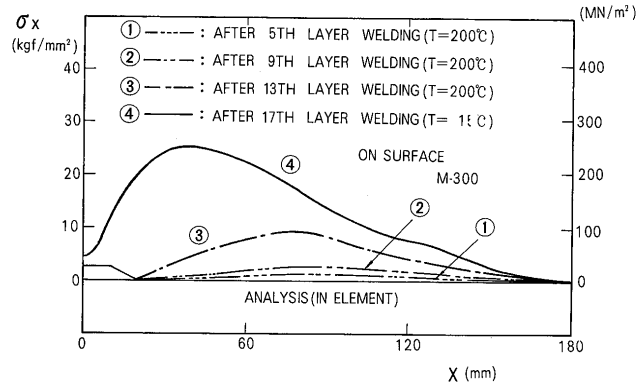

Fig. 14 (a) Transverse welding transient stresses (σ_X) on the top surface (M-300)

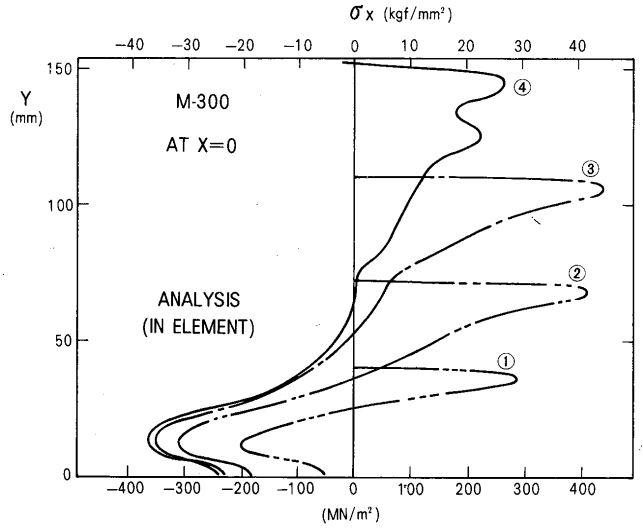

Fig. 14 (b) Transverse welding transient stresses (σ_X) at the cross section (M-300, AT X=0)

stresses, it is considered unnecessary, because the largest tensile stress which appears just below the newest layer decreases as welding proceeds.

4-2 Residual stresses and delayed cracking

In relation to delayed cracks and SR cracks, the location of the largest residual stress is very important. On the finishing bead of the specimen, the residual stresses are in tension but are small, and the largest on the top surface is about 20 mm away from the toe of weld. The largest residual stress in the cross section appears just below the finishing bead. This is also the largest in the whole specimen. (The special features of the residual stress distributions are discussed in Appendix II.)

It is difficult to judge from the residual stresses that delayed cracking initiates at the toe of weld, since the residual stresses are small there. Referring to information about cold cracks and SR cracks which have been reported so far, it is inferred that the cracking is caused by the large tensile stress and the location of the initiation is at several layers below the vicinity of the toe of weld.

4-3 Conditions of annealing and reduction of residual stresses

From the measured and analytical results, it is found that the welding residual stress is relieved fairly at the heating stage, when the heating rate is 30~100°C/hr. and holding temperature is 650°C. While reduction of the stress at the holding stage is comparatively small.

In contrast with this, judging from the results of the annealing for specimen MSR-200-1 (30°C/hr., 600°C, no holding) and the relaxation test at several constant temperatures (500°C to 650°C) in Fig. 11, a heat treatment with annealing temperature of 550°C can not be expected to reduce a large amount of residual stresses, even if the holding time is somewhat long.

5. Concluding remarks

In this study the authors have both theoretically and experimentally investigated welding stresses induced during multipass welding and also the reduction of the welding residual stresses by stress relief annealing on very thick models, which are idealizations of joints between the cylinder and the head of a cylindrical pressure vessel.

To this theoretical analysis, the thermal elastic-plastic creep theory based on F.E.M. has been applied. Although the authors have idealized the properties of metal and simplified the analysis to a certain extent, the theoretical results closely coincide with the experimental results. This coincidence assures applicability of the method adopted in this study.

A summary of important information obtained is shown below.

(1) The largest transient stress (σ_X) during welding always appears just below the weld metal of the newest layer. But as the layers of weld metal are piled up, this stress is relieved gradually and becomes compressive stress in the vicinity of the center of the specimen. This implies that the application of intermediate annealing for the sole purpose on reducing welding residual stresses is unnecessary.

(2) In the transverse welding residual stress (σ_X) distribution, the location of the largest tensile stress on the top surface is about 20 mm away from the toe of weld, and the largest for the whole specimen is just below the finishing bead. Judging from the residual stresses and available information about cracks in actual structures, delayed cracks do not initiate at the toe of weld on the surface, but do initiate several

layers below it.

(3) The effectiveness of stress relief annealing depends greatly on the annealing temperature. In the case of the material (2¼Cr-1Mo) furnished in this study, most of residual stresses are relieved at the heating stage with heating rate of 30°C/hr. to 100°C/hr. if the annealing temperature is 650°C, but if the annealing temperature is 550°C, annealing is not effective even with a longer holding time.

Acknowledgement

The authors would like to thank T.Fukada, Researcher of Central Research Laboratory of Kobe Steel Co., Ltd., for his help with the experimental work and M. Tanigawa, Graduate Student of Osaka Univ., for helpful with the theoretical analysis of the stress relief annealing.

References

1) Ueda, Y. and Yamakawa, T., "Analysis of Thermal Elastic-Plastic Stress and Strain during Welding by Finite Element Method", Trans. of JWS (the Japan Welding Society), Vol. 2, No. 2, 1971, pp90-100; IIW (International Institute of Welding) Doc. X-616-71; and Journal of JWS, Vol. 42, No. 6, 1973, pp567-577 (in Japanese)

2) Ueda, Y. and Fukuda, K., "Analysis of Welding Stress Relieving by Annealing Based on Finite Element Method", IIW Doc. X-773-75; Trans. of JWRI (the Welding Research Institute of Osaka Univ., Japan) Vol. 4, No. 1, 1975, pp34-45; and Journal of JWS, Vol. 44, No. 11, 1975, pp902-908 (in Japanese)

3) Ueda, Y., Takahashi, E., Fukuda, K. and Nakacho, K., "Transient and Residual Stresses in Multi-Pass Welds", IIW Doc. X-698-73; Trans. of JWRI, Vol. 3, No. 1, 1974, pp56-67; and Journal of JWS, Vol. 44, No. 6, 1975, pp465-474 (in Japanese)

4) Ueda, Y., Takahashi, E., Fukuda, K., Sakamoto, K. and Nakacho, K., "Transient and Residual Stresses from Multi-pass Weld in Very Thick Plates and Their Reduction from Stress Relief Annealing", Proceedings of Third International Conference on Pressure Vessel Technology, Japan, 1977, (to be published)

APPENDIX I

Creep Strain Increment Based on Strain-Hardening Creep Law

1. Creep flow laws

As mentioned in Section 3.1, creep behavior of the material (2¼Cr-1Mo steel) is well described by the strain-hardening creep law below 575°C and the power creep law above 575°C. According to the power creep law, stress-strain relation including creep strain has already been obtained. So, the creep strain increment which obeys the strain-hardening creep law will be discussed as follows.

Creep strain induced in an uniaxial creep test can be expressed as,

$$\varepsilon^c = A\,\sigma^\gamma t^m \tag{A.1}$$

The creep strain rate at constant temperature and in constant stress state is calculated from Eq. (A. 1) and yields

$$\dot{\varepsilon}^c = mA\,\sigma^\gamma\, t^{m-1} \tag{A.2}$$

If time t is eliminated from the above two equations (A.1) and (A.2), the following equation may be obtained.

$$\dot{\varepsilon}^c = mA^{\frac{1}{m}}\,\sigma^{\frac{\gamma}{m}}(\varepsilon^c)^{1-\frac{1}{m}} \tag{A.3}$$

When temperature and stress are variables, Eqs. (A.1), (A.2) and (A.3) are called basic equations of the total strain creep law, of the time-hardening law and of the strain-hardening law, respectively.

When the strain-hardening law is used, the material constant m is generally less than unity. Then, at the moment of initiation of creep strain, creep strains may be zero and creep strain rates happen to be calculated as infinite from Eq. (A.3). Therefore, direct application of Eq. (A.3) is not appropriate for the analysis. In order to apply the incremental theory, creep strain increments should be represented by a linear function of stresses and strains.

In order to satisfy this demand, the authors have developed a method to analyse creep behaviors of the strain-hardening type. In the following, the method and the procedure for the analysis are described.

2. Analytical method and procedure for creep behaviors of the strain-hardening type

It should be noted that the strain-hardening law (Eq. (A.3)) is developed as a solution of the simultaneous equations of the time-hardening law (Eq. (A.2)) and the total strain one (Eq. (A.1)), regarding time t as a parameter. Therefore, Eqs. (A.1) and (A.2) are the basic equations for Eq. (A.3) and these equations can be used in spite of applying Eq. (A.3) directly. When the incremental theory is applied, the following method is useful.

First, Eq. (A.2) is regarded as a basic equation and used for the analysis during a certain small time increment dt ($t_{eq} \leqq t \leqq t_{eq} + dt$), where t_{eq} is equal to zero at the first increment step of the analysis and is determined by Eq. (A.8) at the following steps. In the three-dimensional stress state, creep strain rate is given by the next equation which corresponds to Eq. (A.2).

$$\{\dot{\varepsilon}^c\} = \frac{3}{2\bar{\sigma}}\dot{\bar{\varepsilon}}^c\{\sigma'\} = \frac{3}{2}mA\,\bar{\sigma}^{\gamma-1}\{\sigma'\}t^{m-1} = \frac{3}{2}a\bar{\sigma}^{\gamma-1}\{\sigma'\}t^d \tag{A.4}$$

where $\{\sigma'\}$: deviatric stress vector, $\bar{\sigma}$: equivalent stress

$a = mA$, $d = m-1$

Assuming that a, $\bar{\sigma}$, $\{\sigma'\}$ in Eq. (A.4) vary linearly and constants d and γ don't change in a small time interval dt and integrating this equation during the interval $teq \leqq t \leqq teq + dt$, creep strain increment can be expressed as,

$$\{d\varepsilon^c\} = [C_c]\{d\sigma\} + \{d\hat{\varepsilon}^c\} \quad (A.5)$$

where

$$\{d\hat{\varepsilon}^c\} = \frac{3}{2}(K_1 a + K_2 da)\,\bar{\sigma}^{\gamma-1}\{\sigma'\} \quad (A.6)$$

$$[C_c] = (K_2 a + K_3 da)\bar{\sigma}^{\gamma-1}[Cij] \quad (A.7)$$

$$K_1 = \{(teq + dt)^{d+1} - (teq)^{d+1}\}/(d+1)$$

$$K_2 = (teq+dt)^{d+1}/(d+1) - \{(teq+dt)^{d+2} - (teq)^{d+2}\} / \{(d+1)(d+2)dt\}$$

$$K_3 = (teq+dt)^{d+1}/(d+1) - 2(teq+dt)^{d+2}/\{(d+1)(d+2)dt\} + 2\{(teq+dt)^{d+3} - (teq)^{d+3}\}/\{(d+1)(d+2)(d+3)(dt)^2\}$$

$C_{11} = H\sigma_x'\sigma_x' + 1$ $\quad C_{12} = H\sigma_x'\sigma_y' - 1/2$

$C_{13} = H\sigma_x'\sigma_z' - 1/2$ $\quad C_{14} = 2H\sigma_x'\tau_{yz}$

$C_{15} = 2H\sigma_x'\tau_{zx}$ $\quad C_{16} = 2H\sigma_x'\tau_{xy}$

$C_{22} = H\sigma_y'\sigma_y' + 1$ $\quad C_{23} = H\sigma_y'\sigma_z' - 1/2$

$C_{24} = 2H\sigma_y'\tau_{yz}$ $\quad C_{25} = 2H\sigma_y'\tau_{zx}$

$C_{26} = 2H\sigma_y'\tau_{xy}$ $\quad C_{33} = H\sigma_z'\sigma_z' + 1$

$C_{34} = 2H\sigma_z'\tau_{yz}$ $\quad C_{35} = 2H\sigma_z'\tau_{zx}$

$C_{36} = 2H\sigma_z'\tau_{xy}$ $\quad C_{44} = 4H\tau_{yz}\tau_{yz} + 3$

$C_{45} = 4H\tau_{yz}\tau_{zx}$ $\quad C_{46} = 4H\tau_{yz}\tau_{xy}$

$C_{55} = 4H\tau_{zx}\tau_{zx} + 3$ $\quad C_{56} = 4H\tau_{zx}\tau_{xy}$

$C_{66} = 4H\tau_{xy}\tau_{xy} + 3$ $\quad C_{ij} = C_{ji}$ $(i, j = 1 \sim 6)$

$H = 9(\gamma - 1)/(4\bar{\sigma}^2)$

da: change of a due to temperature increment dT in a small time increment dt

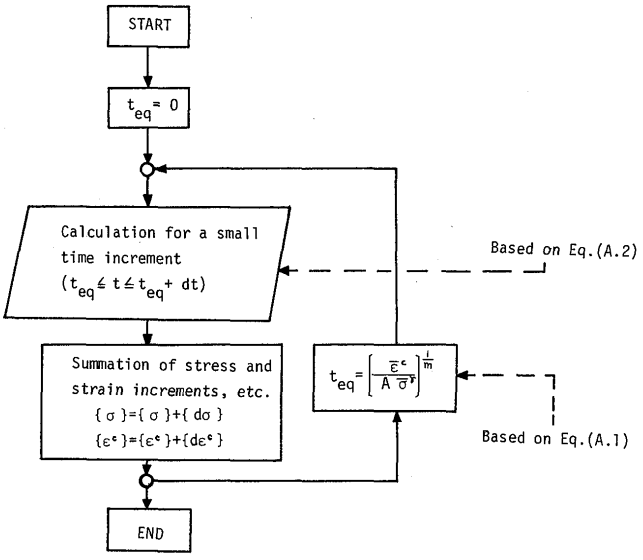

Fig.A Incremental procedure for analysis of creep behaviors of strain-hardening type

After the analysis may be conducted during this increment, and the total stresses and strains are obtained by adding these incremental values to the previous ones, the time, teq for the following incremental step is determined by the next equation which corresponds to Eq. (A.1).

$$teq = \left[\frac{\bar{\varepsilon}^c}{A\bar{\sigma}^\gamma}\right]^{\frac{1}{m}} \quad (A.8)$$

where $\bar{\varepsilon}^c$: equivalent creep strain

This procedure is illustrated in Fig. A.

APPENDIX II

Features of Residual Stress Distributions

The residual stress (σ_x) distributions possess two features;

(1) On the surface of the specimen, the largest tensile stress is produced not on the surface of the finishing bead, but about 20mm away from the toe of weld.

(2) In the stress distribution along the Y axis, two maximum values appear just below the finishing bead and several layers below that.

There should be reasons for these two features. First, the feature (1) will be discussed. Usually, in multipass welds, contraction of the new weld metal and HAZ of the newest pass is restrained by the region surrounding it. The restraint is progressively more severe forward the bottom. While the surface is much less restrained. This tendency becomes even more marked in the finishing layer. Accordingly, the stresses on the surface of the finishing bead must be smaller than those stresses just below the surface. In addition, the temperature of the weld metal including the narrow region of the adjoining plate is high at the completion of multipass welding and the isothermal lines of 200°C are almost parallel to the Y axis. As the temperature decreases, the contraction of these portions in the direction of thickness produces local bending which induces compressive stresses on the surface of the finishing bead. These additional stresses further reduce the tensile stresses mentioned above.

Next, feature (2) will be discussed. The above explanation suggests that the tensile stress in the weld metal, that is produced by its contraction, becomes smaller approaching the top surface, and the largest is found at several layers below the top surface. On the other hand, it is evident from the transient stress distribution that the largest transient stress is always produced just below the newest layer. In the case of the finishing welding, this largest transient stress just below the finishing bead remains as the largest residual stress since no more bead is put on. Accordingly, there are the above mentioned two points where maximum values appear in the residual stress distribution along the Y axis.